Received: 25 October 2022 | Accepted: 26 June 2023

DOI: 10.1097/HEP.0000000000000553

ORIGINAL ARTICLE

OPEN

Multiomics identifies metabolic subtypes based on fatty acid degradation allocating personalized treatment in hepatocellular carcinoma

Binghua Li[1,2] | Yunzheng Li[1] | Huajun Zhou[3] | Yanchao Xu[4] | Yajuan Cao[1] | Chunxiao Cheng[5] | Jin Peng[1] | Huan Li[1] | Laizhu Zhang[1] | Ke Su[1] | Zhu Xu[1] | Yue Hu[6] | Jiaming Lu[7] | Yijun Lu[1] | Liyuan Qian[8] | Ye Wang[1] | Yuchen Zhang[1] | Qi Liu[1] | Yuanyuan Xie[1] | Sheng Guo[3] | Wajahat Z. Mehal[2] | Decai Yu[1,4,5]

[1]State Key Laboratory of Pharmaceutical Biotechnology, Division of Hepatobiliary and Transplantation Surgery, Department of General Surgery, Nanjing Drum Tower Hospital, The Affiliated Hospital of Nanjing University Medical School, Nanjing, China

[2]Department of Internal Medicine, Section of Digestive Diseases, Yale University School of Medicine, New Haven, Connecticut, USA

[3]Department of Data Science & Bioinformatics, Crown Bioscience Inc., Suzhou, Jiangsu, China

[4]Division of Hepatobiliary and Transplantation Surgery, Department of General Surgery, Nanjing Drum Tower Hospital Clinical College of Jiangsu University, Nanjing, China

[5]Division of Hepatobiliary and Transplantation Surgery, Department of General Surgery, Affiliated Drum Tower Hospital, Nanjing University of Chinese Medicine, Nanjing, China

[6]Biobank of Nanjing Drum Tower Hospital, Department of Pathology, The Affiliated Hospital of Nanjing University Medical School, Nanjing, Nanjing, China

[7]Department of Radiology, The Affiliated Drum Tower Hospital, Medical School of Nanjing University, Nanjing, China

[8]Department of Hepatobiliary and Pancreatic Surgery, The First People's Hospital of Changzhou, The Third Affiliated Hospital of Soochow University, Changzhou, China

Correspondence
Wajahat Z. Mehal, Department of Internal Medicine, Section of Digestive Diseases, Yale University School of Medicine, Yale New Haven Hospital, 20 York Street, New Haven, CT 06520, USA.
Email: wajahat.mehal@yale.edu

Decai Yu, State Key Laboratory of Pharmaceutical Biotechnology, Division of Hepatobiliary and Transplantation Surgery, Department of General Surgery, Nanjing Drum Tower Hospital, The Affiliated Hospital of Nanjing University Medical School, Zhongshan Road 321, Nanjing 210008, China.
Email: yudecai@nju.edu.cn

Abstract

Background and Aims: Molecular classification is a promising tool for prognosis prediction and optimizing precision therapy for HCC. Here, we aimed to develop a molecular classification of HCC based on the fatty acid degradation (FAD) pathway, fully characterize it, and evaluate its ability in guiding personalized therapy.

Approach and Results: We performed RNA sequencing (RNA-seq), PCR-array, lipidomics, metabolomics, and proteomics analysis of 41 patients with HCC, in which 17 patients received anti-programmed cell death-1 (PD-1)

Abbreviations: CPTAC, Clinical Proteomic Tumor Analysis Consortium; FAD, fatty acid degradation; FFA, free fatty acid; ICI, immune checkpoint inhibitor; ICGC, International Cancer Genomics Consortium; KEGG, Kyoto Encyclopedia of Genes and Genomes; LIMORE, Liver Cancer Model Repository; OS, overall survival; PDX, patient-derived xenograft; PD-1, programmed cell death-1; RNA-seq, RNA sequencing; RTV, relative tumor volume; scRNA-seq, single-cell RNA sequencing; TACE, transarterial chemoembolization; T + A, atezolizumab plus bevacizumab; TCGA, The Cancer Genome Atlas.

Binghua Li, Yunzheng Li, and Huajun Zhou contributed equally.

The study was approved by the Research Ethics Committee of Drum Tower Hospital (ChiCTR1900026022), and written informed consent was obtained from each patient. All animal studies were performed following a protocol approved by the Institutional Ethics Committee for Clinical Research and Animal Trials of Drum Tower Hospital.

Supplemental Digital Content is available for this article. Direct URL citations are provided in the HTML and PDF versions of this article on the journal's website, www.hepjournal.com.

therapy. Single-cell RNA sequencing (scRNA-seq) was performed to explore the tumor microenvironment. Nearly, 60 publicly available multiomics data sets were analyzed. The associations between FAD subtypes and response to sorafenib, transarterial chemoembolization (TACE), immune checkpoint inhibitor (ICI) were assessed in patient cohorts, patient-derived xenograft (PDX), and spontaneous mouse model ls. A novel molecular classification named F subtype (F1, F2, and F3) was identified based on the FAD pathway, distinguished by clinical, mutational, epigenetic, metabolic, and immunological characteristics. F1 subtypes exhibited high infiltration with immunosuppressive microenvironment. Subtype-specific therapeutic strategies were identified, in which F1 subtypes with the lowest FAD activities represent responders to compounds YM-155 and Alisertib, sorafenib, anti-PD1, anti-PD-L1, and atezolizumab plus bevacizumab (T + A) treatment, while F3 subtypes with the highest FAD activities are responders to TACE. F2 subtypes, the intermediate status between F1 and F3, are potential responders to T + A combinations. We provide preliminary evidence that the FAD subtypes can be diagnosed based on liquid biopsies.

Conclusions: We identified 3 FAD subtypes with unique clinical and biological characteristics, which could optimize individual cancer patient therapy and help clinical decision-making.

INTRODUCTION

Liver cancer is ranked as the sixth most common neoplasm and the fourth leading cause of cancer death, in which HCC accounts for about 85%–90%.[1] HCC displays high complexity and heterogeneity of molecular phenotypes. Molecular classification is a promising tool for optimizing prognosis prediction and precision medicine for an individual patient.[2] Recent advances in multiomics have led to unprecedented efforts in characterizing the molecular classifications of HCC based on histopathological, mutational, transcriptomic, and epigenetic landscape generated from microarray, RNA sequencing (RNA-seq), and proteomics platforms, leading to the definition of several subgroups from chromosomal, mutational, metabolic, and immunological perspectives.[3–8] Although these classifications depict parts of the molecular mechanisms and stratify patient prognosis, classification based on a single signaling or metabolic pathway that could guide personalized therapy is still lacking.

Dysregulation of fatty acid (FA) metabolism has increasingly emerged as a hallmark of cancer cells.[9] Cancer cells frequently exhibit alterations in FA metabolism to sustain growth and proliferation, fulfill energy requirements, provide cellular building blocks for membrane formation, and produce signaling molecules or post-translational modifications.[10] FAs can be degraded by means of different pathways including α-, β-, and ω-oxidation, occurring in the mitochondria and the peroxisomes.[11] A growing body of evidence suggests that the enhanced de novo FA synthesis is an important feature of HCC.[12] By contrast, fatty acid degradation (FAD) in cancer cells has received less attention. It is reported that CTNNB1-mutated HCC oxidized FAs as a source of energy in the metabolic adaptation under the control of the transcription factor PPARα.[13] However, a systematic evaluation of FAD in tumors especially in HCC is still in need of further investigation.

The treatment options of HCC principally depend on the tumor stages, in which patients with early-stage HCC tumors are the first candidates for resection, local ablation or transplantation, whereas patients at intermediate stages are preferred candidates for transarterial chemoembolization (TACE) and those with advanced disease benefit from systemic therapies including immunotherapy [anti-programmed cell death-1 (PD-1) and anti-PD-L1) and targeted therapy (sorafenib, lenvatinib, and regorafenib).[14] The combination of atezolizumab with bevacizumab (T + A) is currently the first-line treatment, since it confers a superior survival benefit compared to sorafenib.[15] However, patients belonging to the same HCC stage can respond differently to the same treatment, highlighting the urgent need to identify biomarkers for clinical decision-making.

In this study, we comprehensively surveyed the expression profile and prognostic value of FAD pathway and identified a FAD-based molecular classification of HCC which we termed F subtype (F1, F2, and F3) in 9 independent data sets generated by various platforms of over 1500 patients. We further explored the genomic, epigenetic, metabolic, signaling, and immunological landscape of the FAD subtypes and proposed the subtype-specific therapeutic strategies.

METHODS

Clinical sample acquisition

Samples were collected retrospectively from the Biobank of Nanjing Drum Tower Hospital between January 2019 and June 2021. Seventeen patients who were available with clinical responses to anti-PD-1 therapy and biopsy or surgical resection specimens were included in this study (8 responders and 9 nonresponders). To ensure there was enough sample size for clustering analysis, we also enrolled some surgically resected primary tumor tissues and paired nontumor liver tissues from patients with HCC who did not receive anti-PD1 blockade with different tumor stages. In total, 69 samples from 44 patients were subjected to transcriptomic and lipidomic analyses. Three samples did not pass the quality control for RNA-seq and 6 samples did not pass the quality control for lipidomics analysis due to tissue degradation or limited tissue amount, thus being ruled out from the study. As a result, 41 patients performed RNA-seq analysis and 40 patients performed lipidomics. The serum of the 41 patients was subjected to metabolomics and proteomics analysis. The detailed clinical data and the baseline patient characteristics for our cohort are summarized in Supplemental Tables S1, http://links.lww.com/HEP/H916 and S5, http://links.lww.com/HEP/H917. The raw lipidomics data are cataloged in Supplemental Table S2, http://links.lww.com/HEP/H916. Each sample was assigned a new research ID, and the patient's name or medical record number used during hospitalization was deidentified. All patients provided written informed consent, and the study design was consistent with the Declarations of Helsinki and Istanbul. The protocol of the study was approved by the Research Ethics Committee of Drum Tower hospital (ChiCTR1900026022).

Animal models

Mice were obtained from the Model Animal Research Center of Nanjing University (Nanjing, China). All experimental procedures using animals were in accordance with the ARRIVE (Animals in Research: Reporting In Vivo Experiments) statement and the guidelines provided by the Animal Ethics Committee of the Affiliated Drum Tower Hospital of Medical School of Nanjing University.

Public data collection and preparation

In total, 59 publicly available data sets were reanalyzed in this study, including 37 microarray data sets, 15 RNA-seq data sets, 2 metabolomics data sets, 2 proteomics data sets, and 3 single-cell RNA sequencing (scRNA-seq) data sets. All the data sets used in this study are summarized in Supplemental Table S3, http://links.lww.com/HEP/H916. The gene signatures for previous HCC classifications are listed in Supplemental Table S4, http://links.lww.com/HEP/H916. The clinical characteristics of the included publicly available cohorts are listed in Supplemental Table S6, http://links.lww.com/HEP/H917.

Statistical analysis

The quantitative data were analyzed with Student's t-test, Mann–Whitney *U* test or Kruskal-Wallis test with post hoc Dunn test. The qualitative data were analyzed with Pearson chi-squared or Fisher exact test as appropriate. Survival curves were estimated by the Kaplan-Meier method. The log-rank test was used to determine the statistical differences between survival curves. Statistical analysis and data visualization were carried out using the R/Biocoductor software packages.

Full and detailed descriptions of research materials and experiment methods are provided in online Supporting Information.

RESULTS

Transcriptomics and lipidomics depict the characteristics of FAD pathway in HCC

We have identified all the prognostic genes in HCC.[16] Kyoto Encyclopedia of Genes and Genomes analysis highlighted the FAD pathway (Figure 1A), which consists of 42 genes that function in mitochondrial β-oxidation, peroxisomal ω-, and β-oxidation (Figure 1B). Most of the FAD genes were significantly downregulated in tumor tissues and positively correlated with the prognosis of patients in multiple cancer types (Figure 1B, Supplemental Figure S1, http://links.lww.com/HEP/H917). RNA-seq validated the downregulation of FAD genes in our cohort ($n = 41$). Correspondingly, the content of free fatty acids (FFAs) was increased in tumor tissues as measured by lipidomics and metabolomics (Figure 1C, Supplemental Figure S2, http://links.lww.com/HEP/H917).

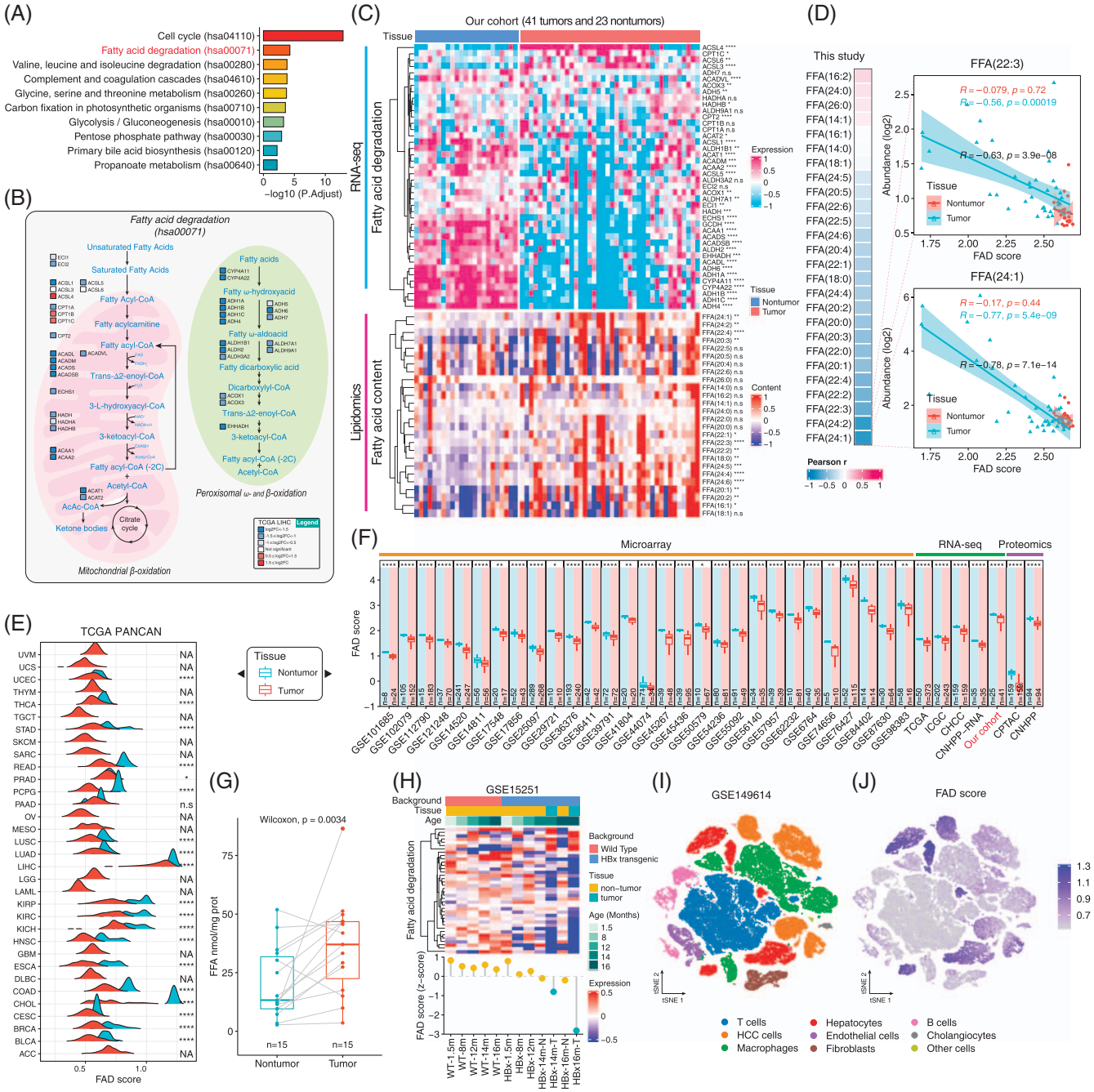

FIGURE 1 FAD is downregulated in multiple cancers and correlated with fatty acid content in tumors. (A) KEGG analysis of the prognostic genes in TCGA LIHC data set. (B) Schematic diagram showing the FAD pathway and the expression pattern of FAD genes in HCC and adjacent nontumor samples based on TCGA LIHC data set. (C) The expression pattern of FAD genes (upper panel) and the content of FFAs (lower panel) in tumor versus nontumor tissue based on our cohort. (D) The correlations between FAD score and FFAs content based on our data. The scatter plots of 2 representative FFAs were shown in right panel. (E) The expression pattern of FAD score in TCGA PANCAN data set. The abbreviations can be found in the supplementary information. (F) The expression pattern of FAD score in HCC tumor tissues and nontumor tissues based on microarray, RNA-seq, and proteomics data sets. (G) The contents of FFAs in 15 pairs of HCC tumor and nontumor tissues. (H) The expression pattern of FAD pathway during hepatocarcinogenesis in an HBx-induced mouse HCC model. The FAD score for each sample was shown in the lower panel. (I) t-SNE plot for the cell type identification of 71,915 high-quality single cells for 10 patients with HCC from 4 relevant sites: primary tumor, portal vein tumor thrombus (PVTT), metastatic lymph node, and nontumor liver. (J) The expression pattern of FAD score in different cell types. *$p < 0.05$; **$p < 0.01$; ***$p < 0.001$; ****$p < 0.0001$. Abbreviations: FAD, fatty acid degradation; FFA, free fatty acid; KEGG, Kyoto Encyclopedia of Genes and Genomes; LIHC, liver hepatocellular carcinoma; TCGA, The Cancer Genome Atlas; WT, wild type.

We calculated the FAD score to represent the metabolic activity of FAD pathway using the ssGSEA method. The FAD score was inversely correlated with most FFAs in our cohort (Figure 1D, Supplemental Figure S3, http://links.lww.com/HEP/H917), which was further validated by a breast cancer data set (Supplemental Figure S4, http://links.lww.

com/HEP/H917). These data suggest that the expression of FAD genes and the FAD score do reflect the metabolic activities of FAD pathway and the content of FFAs. The FAD score was high in normal liver and kidney and was downregulated in most tumors compared to their nontumor counterparts (Figure 1E), which was further validated by one scRNA-seq data set (Supplemental Figure S5A, B, http://links.lww.com/HEP/H917). The FAD score was significantly reduced in HCC as validated in 36 data sets comprising 5800 samples with differing etiologies (Figure 1F), which was consistent with the increasing concentration of total FFAs in tumor tissues (Figure 1G). Besides, the expression level of FAD genes decreased in multiple mouse HCC models (Figure 1H, Supplemental Figure S5C, D, http://links.lww.com/HEP/H917). Finally, scRNA-seq validated that HCC clusters had lower FAD score levels than normal hepatocyte clusters (Figure 1I, J). Notably, scRNA-seq also revealed cluster-to-cluster heterogeneity of FAD score in HCC cells, implying that enhanced stratification of patients was needed (Figure 1J).

Identification and validation of a FAD-based subtype of HCC and its clinicopathologic correlations

We further evaluated the prognostic potentiality of FAD score in HCC. FAD score was positively correlated with overall survival (OS) and recurrence-free survival in multiple cohorts (Supplemental Figure S6, http://links.lww.com/HEP/H917). Clinical parameters that reflect biological aggressiveness such as advanced clinical stage, larger tumor size, and higher AFP level were correlated with lower FAD score (Supplemental Figure S7, http://links.lww.com/HEP/H917 and Supplemental Table S7, http://links.lww.com/HEP/H917). Univariate and multivariate analyses demonstrated that FAD score was the only independent predictor of OS in all data sets after adjusting for prognosis-related clinical variables (Figure 2A, Supplemental Table S8, http://links.lww.com/HEP/H917).

Unsupervised consensus clustering was performed based on the expression pattern of the 42 FAD genes. patients with HCC in our cohort were clustered into 3 subgroups, which we termed the F subtypes (initial of FA). F1, F2, and F3 subtypes represent low, intermediate, and high expression levels of FAD genes, respectively (Figure 2B upper panel). Likewise, lipidomics showed that F1 subtypes had more FFAs than other subtypes (Figure 2B middle panel). Conversely, the contents of other lipids such as TAG and DAG were much lower in F1 subtypes (Supplemental Figure S8, http://links.lww.com/HEP/H917). The F1 subtypes were associated with higher AFP levels and advanced tumor stages in our cohort (Figure 2B top panel, Supplemental Table S9, http://links.lww.com/HEP/H917). F1, F2, and F3 subtypes exhibited the shortest, median, and longest OS and recurrence-free survival time, respectively (Figure 2C). The existence and robustness of the FAD subtypes were further validated in eight independent data sets generated from microarray, RNA-seq, and proteomics platforms comprising nearly 1500 patients with diverse HCC etiologies and stages of the disease (Supplemental Figure S9, http://links.lww.com/HEP/H917). Clinicopathologic factors of aggressive behavior such as larger tumor size were more prominent in F1 subtypes (Supplemental Figure S9, http://links.lww.com/HEP/H917 and Supplemental Table S10, http://links.lww.com/HEP/H917). The prognostic value of FAD subtypes was further validated in 5 independent cohorts (Figure 2D–H). Notably, after stratifying patients according to tumor stage, FAD subtypes still strongly correlated with patient prognosis regardless of tumor stages, supporting the superior prognostic power of molecular features within FAD subtypes (Supplemental Figure S10, http://links.lww.com/HEP/H917). We further designed a FAD-based PCR-array considering its advantages for easy-access, cost-effective, and time-saving, which almost replicated the RNA-seq results (Figure 2B below panel), indicating the PCR-array might have practical value for clinical application. Taken together, these results demonstrated that FAD classification is stable across data sets and correlated to clinicopathologic indexes with prognostic values.

Research has established multiple molecular classifications of HCC, including Hoshida et al,[17] Chiang et al,[18] Lachenmayer et al,[19] Boyault et al,[20] Lee et al,[21] Coulouarn et al,[22] Jiang et al,[7] Gao et al,[6] Lee et al,[23] Sia et al,[4] and the clusters from The Cancer Genome Atlas (TCGA).[5] The FAD signature had the smallest gene number and had few overlaps with other signatures (Supplemental Figure S11, http://links.lww.com/HEP/H917 and Supplemental Table S4, http://links.lww.com/HEP/H91). The comparison between FAD subtypes and previously curated classifications showed that there were considerable overlaps between the FAD subtypes and other HCC classifications (Figure 2I, J, Supplemental Table S11, http://links.lww.com/HEP/H917), supporting the reliable clustering procedure of the FAD subtypes.

Genomic, epigenetic, metabolic, and signaling landscape in the FAD subtypes for HCC

We further explored the genomic, epigenetic, metabolic, and signaling characteristics of FAD subtypes. F1 and F3 subtypes harbor the highest mutational ratio of TP53 and CTNNB1, respectively, in TCGA and International Cancer Genomics Consortium cohorts (Figure 3A, B, Supplemental Figure S9C1, http://links.lww.com/HEP/H917 and Supplemental Tables S10-2, http://links.lww.com/HEP/H917 and S12, http://links.lww.com/HEP/H917). Copy number variation analysis showed that F1 subtypes had more amplifications in chromosomes 10 and 12, while F3 subtypes had fewer deletions in chromosomes 1p and

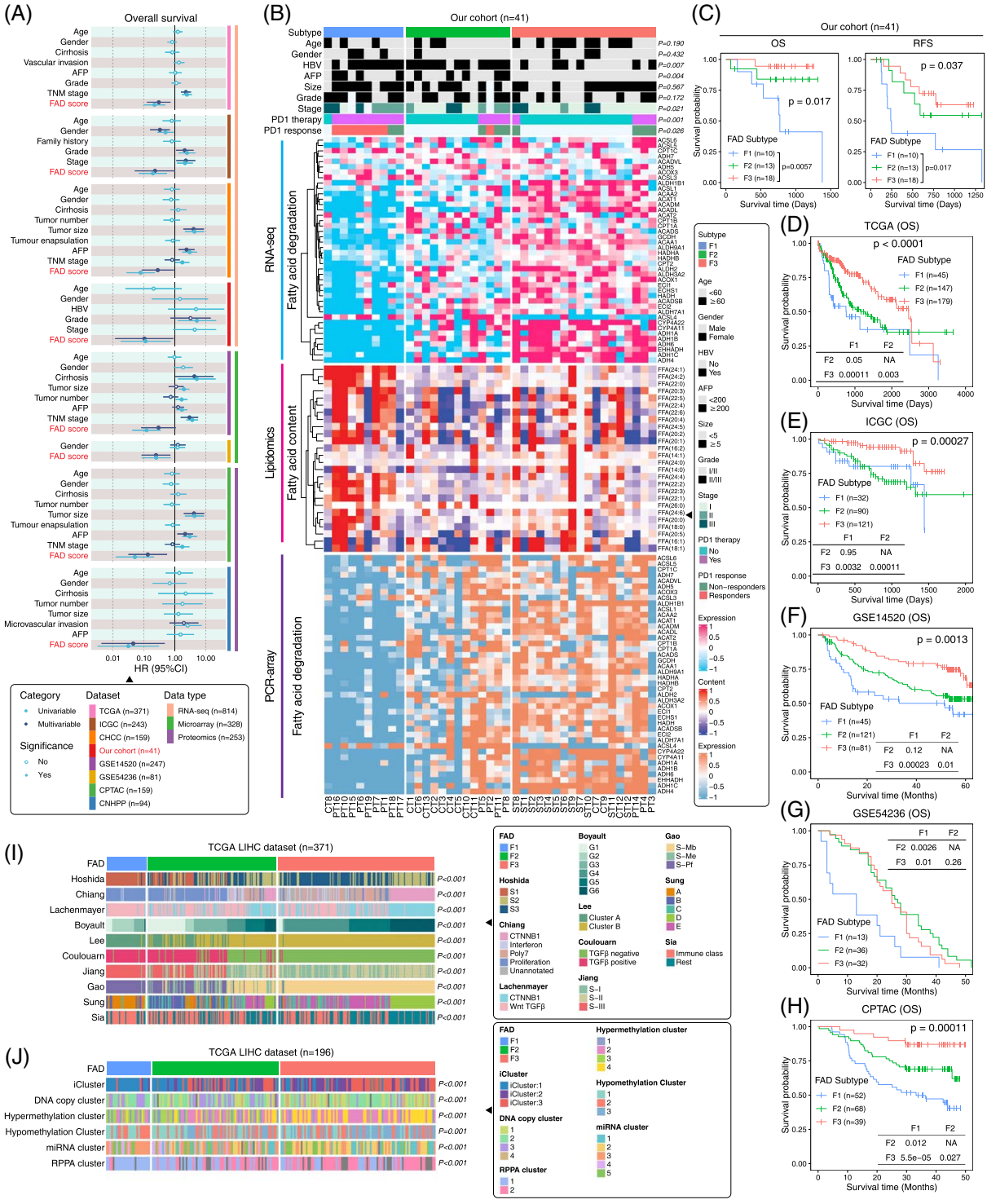

FIGURE 2 Identification and validation of a FAD-based subtype of HCC and its clinicopathologic correlations. (A) Forrest plot of the univariate and multivariate Cox regression analysis of the indicated cohorts. (B) Heatmaps showing the identification of FAD subtypes in our cohort (n = 41). The associations of FAD subtypes with clinical characteristics were annotated in the top panel. The heatmap in the upper panel showed the expression pattern of FAD genes evaluated by RNA-seq. The heatmap in the middle panel displayed the content of fatty acids measured by lipidomics. The heatmap in the lower panel indicated the expression of FAD genes measured by PCR-array. (C) Kaplan-Meier curves of OS and RFS for FAD subtypes in our cohort. (D–H) Kaplan-Meier curves for OS stratified by FAD subtypes in TCGA (D), ICGC (E), GSE14520 (F), GSE54236 (G), and CPTAC (H) data sets. The insets indicated pairwise comparison. (I) Comparisons of the FAD subtypes with 10 previously reported classifications based on TCGA data set. (J) Comparisons of the FAD subtypes to TCGA clusters. Abbreviations: CPTAC, Clinical Proteomic Tumor Analysis Consortium; FAD, fatty acid degradation; ICGC, International Cancer Genomics Consortium; PD-1, programmed cell death-1; TCGA, The Cancer Genome Atlas.

4q (Figure 3C). Epigenetic analysis exhibited a higher methylation rate of FAD genes in F1 subtypes (Figure 3D). The expression of FAD genes was inversely correlated with their methylation levels, indicating that DNA methylation may partly explain the inactivation of FAD pathway in HCC (Figure 3E, Supplemental Figure S12, http://links.lww.com/HEP/H917).

F1 subtypes were distinguished by the significant upregulation of key enzymes in glycolysis, pentose phosphate pathway, nucleic acid, and amino acid metabolism pathway, indicating the increasing demand for energy formation, and macromolecular synthesis (Supplemental Figure S13A, http://links.lww.com/HEP/H917). F1 subtypes had higher activity of TGF-β, NOTCH, and RAS signaling, while F3 subtypes had relatively higher AKT/mTOR pathway activity (Supplemental Figure S13A, http://links.lww.com/HEP/H917). F1 subtypes had the highest glycolysis activity (Figure 3F), whereas F3 subtypes had higher OXPHOS activity compared to F1 and F2 (Figure 3G). FAD classification was applied to HCC cell lines from Liver Cancer Model Repository and Cancer Cell Line Encyclopedia data sets. The frequently used cell lines such as Hep3B, MHCC97H, and SK-Hep-1 belong to F1 subtypes, while HepG2, C3A, and Huh7 were F3 subtypes (Supplemental Figure S14, http://links.lww.com/HEP/H917). Seahorse analysis validated that cell lines in F3 had much higher OXPHOS activity than F1 subtypes (Figure 3H).

Subgroup-specific pathway enrichment analysis revealed distinct molecular features among three FAD subtypes (Figure 3I). F1 subtypes were high in glycolysis, nucleotide metabolism, and proliferative signaling including RAS, TGF-β, NOTCH, and ERK. Conversely, F3 subtypes were enriched in liver-specific metabolic pathways such as xenobiotic, bile acid, and ketone body metabolism, indicating a residual liver function in F3 subtypes. In addition, F3 subtypes had high activity of PI3K/AKT/mTORC, PPAR, and GSK3 pathways. The F2 subtypes resembled a partial mixture of F1 and F3 with intermediate activation in certain metabolic and signaling pathways (Figure 3I).

We then analyzed the expression pattern of HCC biomarkers in FAD subtypes,[6] in which most markers were significantly upregulated and predicted an unfavorable prognosis of HCC. AFP, SPP1, PKM2, THY, and CDK1 were enriched in F1 subtypes, while F3 had high expression of GLUL, GLYATL1, and CPS1, and F2 had high expression of GPC3 (Supplemental Figure S13B–C, http://links.lww.com/HEP/H917). In addition, we applied the FAD subtypes to a scRNA-seq data set. Patients with HCC were divided into 3 subtypes based on the FAD score (Figure 3J, K). Pathway enrichment analysis showed that F1 subtypes were enriched with glycolysis, DNA replication, RAS, MYC, and NOTCH signaling, whereas F3 subtypes had higher activity of liver-specific metabolic pathways such as gluconeogenesis, bile acid metabolism (Figure 3L, Supplemental Figure S15, http://links.lww.com/HEP/H917), which was consistent with the results obtained from bulk RNA-seq. Overall, FAD subtypes represent unique patient subgroups with specific genomic, epigenetic, metabolic, and molecular features that are potentially vulnerable to existing therapeutic agents.

Exploring FAD subtype-specific drugs for HCC

HCC classification enables our understanding of heterogeneity in HCC and could be used to guide personalized therapy.[2] We attempted to unearth subtype-specific vulnerabilities of the FAD classification. To this end, we first started with preclinical drug discovery (Figure 4A). YM-155 and Alisertib were considered as F1-specific drugs as identified by the oncoPredict algorithm using three pharmacogenomic data sets. In contrast, no drug was identified as F3-specific drug using the same criterion (Figure 4B). Most drug targets including the target of YM-155 (BIRC5) and Alisertib (AURKA) were significantly upregulated in F1 subtypes and negatively correlated with FAD score (Figure 4C). The results were further validated in Liver Cancer Model Repository data set (Supplemental Figure S16, http://links.lww.com/HEP/H917), in which the drug resistance of YM-155 and Alisertib was significantly lower in F1 than F3 subtypes (Figure 4D). The proliferation assay showed that F1 cell lines were more susceptible to YM-155 and Alisertib than F3 subtypes (Figure 4E), which presented good agreements with the bioinformatics-based results. Furthermore, YM-155 and Alisertib markedly suppressed the growth of MHCC97H (F1 subtype) rather than Huh7 (F3 subtype) xenograft models (Figure 4F). Overall, these data showed that F1 subtypes were candidates for compounds YM-155 and Alisertib.

FAD subtypes are associated with response to sorafenib and TACE

Next, we assessed the associations between FAD subtypes and first-line treatments in HCC. The patients receiving sorafenib therapy were clustered into FAD subtypes (Figure 5A). F1 patients had the highest response rate to sorafenib, while 90% of the F3 patients were sorafenib nonresponders (Figure 5B). The FAD score in responders was significantly lower than that in nonresponders (Figure 5C) and had good performance in predicting sorafenib response with an AUC of 0.922 (Figure 5D). Consistently, none of the F3 patients respond to sorafenib in IMbrave150 phase 3 trial, although it is not statistically different due to the limited sample size (Supplemental Figure S17A, B, http://links.lww.com/HEP/H917).

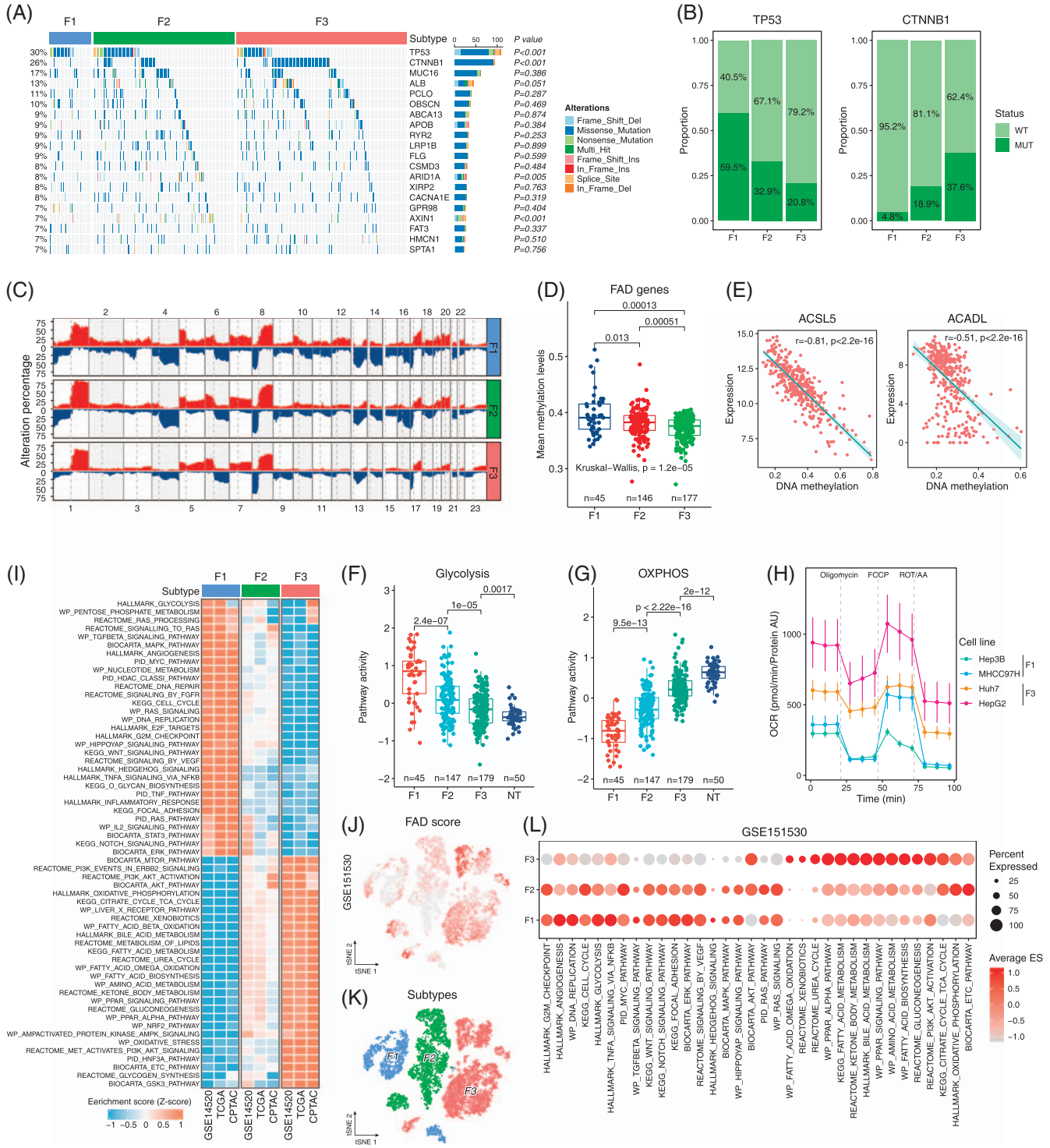

FIGURE 3 Genomic, epigenetic, metabolic, and signaling landscape in the FAD subtypes for HCC. (A) Oncoplot summarizing the distribution of SNVs and INDELs mutational frequency in LIHC data set across the FAD subtypes for the top 20 mutated genes. (B) The percentage of TP53 and CTNNB1 mutation in FAD subtypes. (C) Genomic overview showing the percentage of samples with copy number events among each FAD subtype. Blue represents deletions, red represents gains. (D) Average methylation levels of FAD genes in each FAD subtype. (E) Scatterplots of two representative FAD genes shown to be hypermethylated in HCC. The pathway activity of glycolysis (F) and OXPHOS (G) in different FAD subtypes and nontumor tissues. (H) Seahorse analysis of oxygen consumption rate (OCR) in HCC cell lines from F1 and F3 subtypes. (I) Integrated analysis of differentially activated metabolic and signaling pathways among F1, F2, and F3 based on microarray, RNA-seq, and proteomics data sets. (J) t-SNE plot of the malignant cells in GSE151530 colored by FAD score. (K) Assigning the malignant cells into different FAD subtypes based on FAD score. (L) Dot plot showing the activity of metabolism and signaling pathways across different FAD subtypes in the scRNA-seq data set. Abbreviations: FAD, fatty acid degradation; LIHC, liver hepatocellular carcinoma; TCGA, The Cancer Genome Atlas.

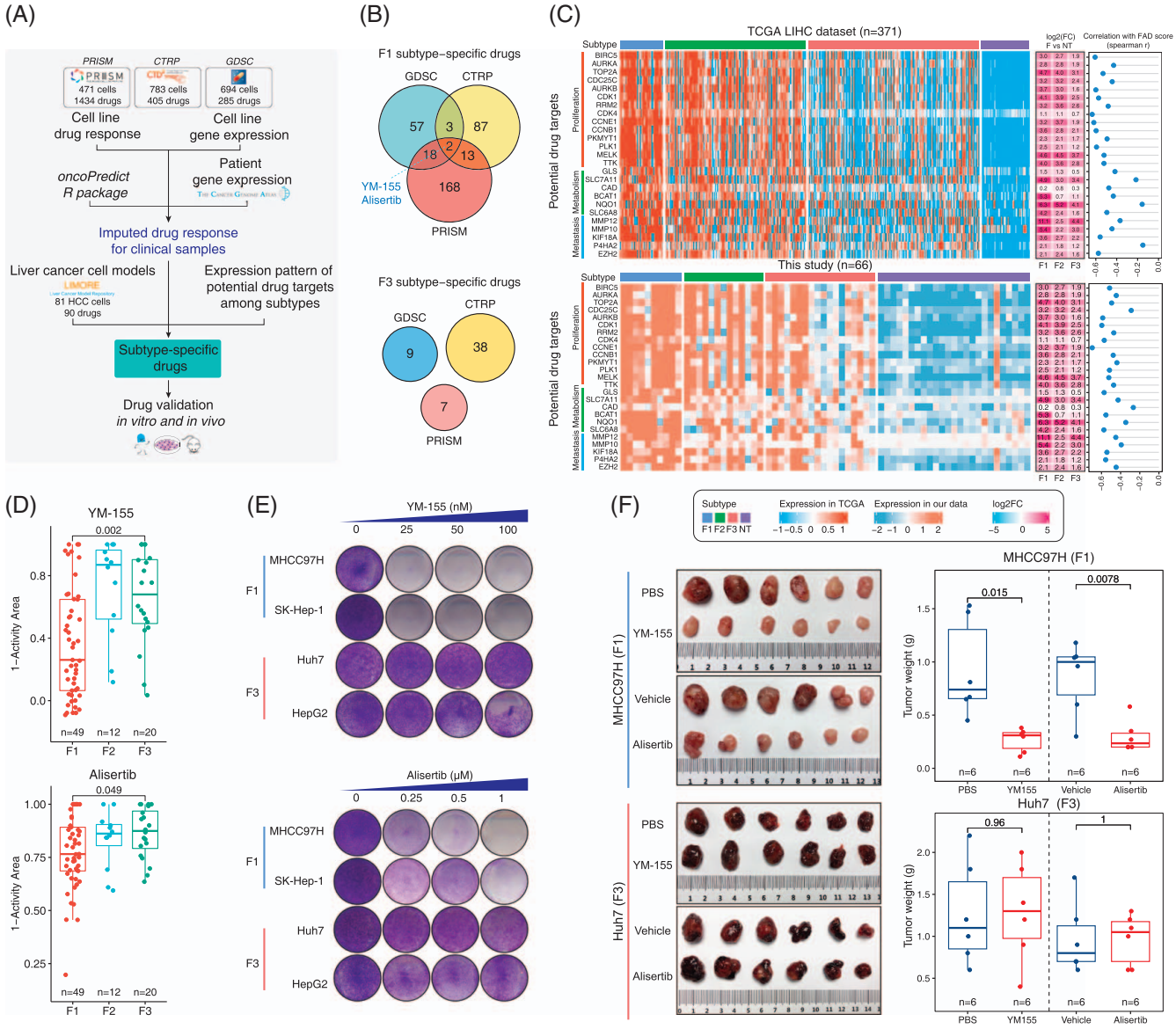

FIGURE 4 Exploring FAD subtype-specific drugs for HCC. (A) Overview of the analysis procedures. (B) Venn diagram summarizing F1 and F3-specific drugs. (C) The expression pattern of potential drug targets in different FAD subtypes and nontumor tissues in TCGA and our data set. The drug target information was curated from the Drug Repurposing Hub. The middle panel shows the log2 fold-change in different subtypes versus nontumor tissues. The right panel shows the correlations between gene expression and FAD score. (D) The drug resistance of YM-155 and Alisertib in F1, F2, and F3 subtypes based on LIMORE database as measured by 1-activity area (AA) values. (E) Long-term colony formation assay showing the response of cell lines from F1 (MHCC97H and SK-Hep-1) and F3 (Huh7 and HepG2) subtypes to YM-155 and Alisertib. (F) Xenograft tumor pictures and tumor weight of indicated MHCC97H and Huh7 cells subcutaneously injected into nude mice followed by YM-155 or Alisertib treatment. Abbreviation: FAD, fatty acid degradation; LIMORE, Liver Cancer Model Repository; TCGA, The Cancer Genome Atlas.

We then used patient-derived xenograft (PDX) models to validate these findings (Figure 5E). FAD classifier was applied to the PDX model cohort (n = 104, Supplemental Figure S17C, http://links.lww.com/HEP/H917), in which 24 PDX models were treated with sorafenib (50 mg/kg) or vectors (Figure 5E). PDX tumors in F1 and F2 were more sensitive to sorafenib than F3 subtypes as measured by AUC ratio (high AUC ratio, high tumor growth rate, Figure 5F, G) and relative tumor volume (high relative tumor volume, high tumor growth rate, Figure 5H, I). The tumor growth was inhibited by sorafenib in F1 rather than F3 subtypes (Figure 5J). Consistently, the sorafenib-resistant mouse spontaneous HCC models had much higher FAD activities than sorafenib-sensitive models (Figure 5K, L). Interestingly, sorafenib treatment leads to an increased expression of FAD genes in vitro and in vivo (Figure 5M, N), implying a shift from the F1 to F3 subtypes.

We noticed that F3 had a higher TACE response rate than F1 subtypes in GSE14520 cohort (Supplemental Figure S9D1, http://links.lww.com/HEP/H917, Table S10-4, http://links.lww.com/HEP/H917). Notably, all patients in F1 subtypes were TACE nonresponders (Figure 5O). The FAD score in TACE responders was much higher than

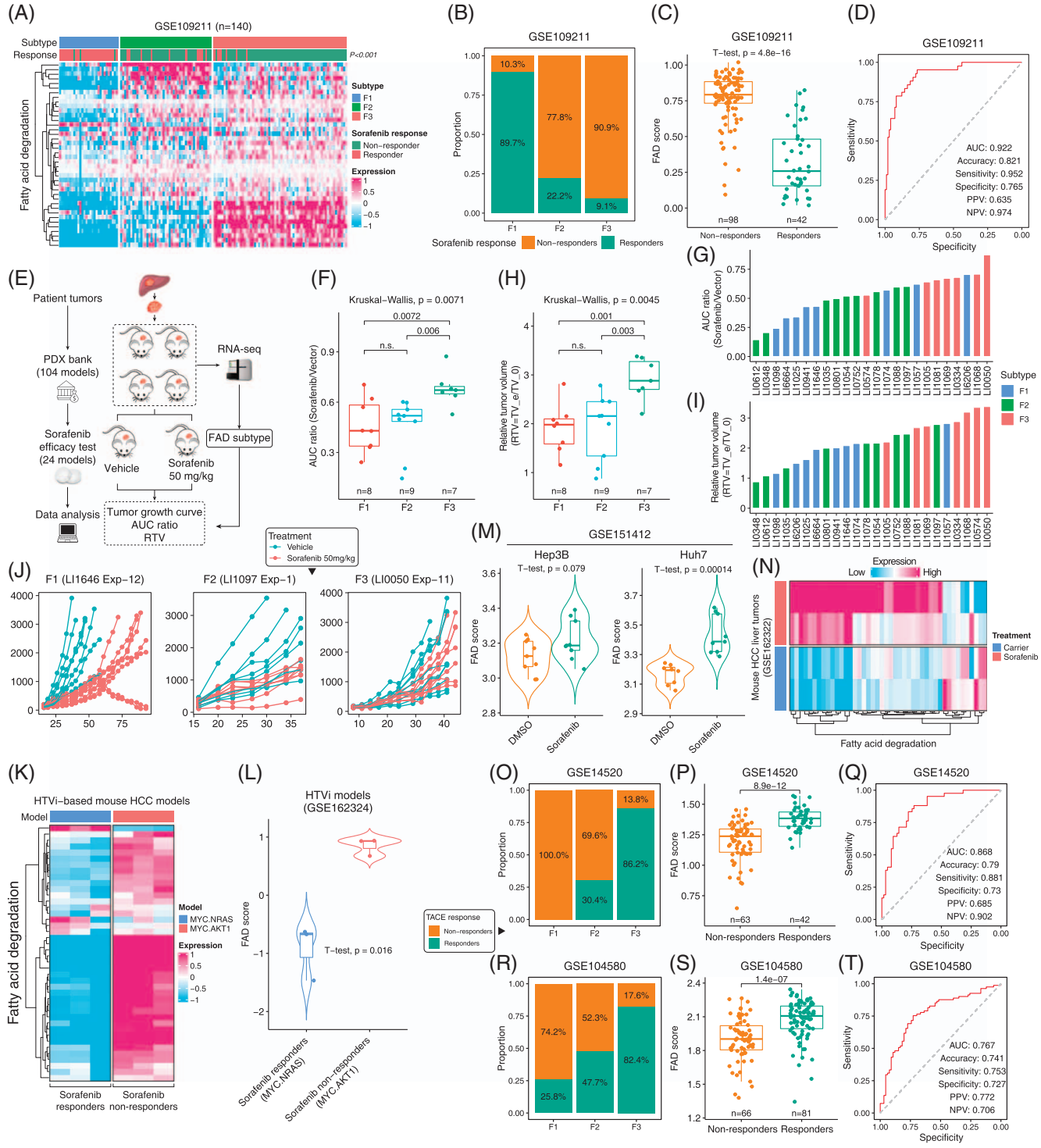

FIGURE 5 FAD subtypes are associated with response to sorafenib and TACE. (A) Heatmap showing the 3 FAD subtypes in GSE109211 data set with sorafenib response available. (B) The percentage of sorafenib responders and nonresponders across FAD subtypes in the indicated data set. (C) Boxplot showing the FAD score in sorafenib responders and nonresponders. (D) AUC showing the performance of the FAD score in predicting sorafenib response. (E) Schematic diagram for the PDX experimental procedure. (F and G) The tumor growth rate of 50 mg/kg sorafenib or vector-treated PDX models in FAD subtypes as shown by AUC ratio. (H and I) The tumor growth rate of 50 mg/kg sorafenib-treated PDX models in FAD subtypes as shown by RTV. (J) Representative tumor growth curves in each FAD subtype. The expression pattern of FAD genes (K) and FAD score (L) in mouse HCC models of sorafenib responders and nonresponders. (M) Sorafenib treatment leads to an increase of FAD score in Hep3B and Huh7 cells. (N) The expression of FAD pathway was much higher in sorafenib-treated tumors than carrier-treated tumors in Myc/NrasG12V mouse HCC model. (O) The percentage of TACE responders and nonresponders across FAD subtypes in patients with HCC from GSE14520. (P) Boxplot showing the FAD score in TACE responders and nonresponders in GSE14520. (Q) AUC showing the performance of the FAD score in predicting TACE response in GSE14520. (R) The percentage of TACE responders and nonresponders across FAD subtypes in GSE104580. (S) Boxplot showing the FAD score in TACE responders and nonresponders in GSE104580. (T) AUC showing the performance of the FAD score in predicting TACE response in GSE104580. Abbreviations: RTV, relative tumor volume; TV_e, tumor volume at the end of study; TV_0, tumor volume before sorafenib administration.

that in nonresponders (Figure 5P) and could predict TACE response with an AUC of 0.868 (Figure 5Q). The difference in TACE response among FAD subtypes was independent of tumor stages (Supplemental Figure S18A, http://links.lww.com/HEP/H917). These results were further validated in an independent data set (Figure 5R–T, Supplemental Figure S18B, C, http://links.lww.com/HEP/H917). Collectively, these data showed that F1 patients were more sensitive to sorafenib, while F3 subtypes are responsive to TACE.

Characterization of the tumor microenvironment (TME) in FAD subtypes of HCC

We first evaluated the expression of immunomodulators across FAD subtypes using four RNA-seq cohorts. F1 subtypes had the highest expression of genes related to co-stimulators, coinhibitors, ligands, receptors, etc. (Supplemental Figure S19A, http://links.lww.com/HEP/H917). The contents of most immune cells and their marker genes were much higher in F1 than other subtypes (Supplemental Figure S19B, C, http://links.lww.com/HEP/H917). There was no difference in tumor mutational burden among FAD subtypes in TCGA and International Cancer Genomics Consortium cohorts (Supplemental Figure S20A, B, http://links.lww.com/HEP/H917). Reanalysis of the scRNA-seq data set revealed that the F1-derived T cells had much higher expression of cytotoxic and exhausted T cell markers, indicating a highly immune infiltrated and actively immune-suppressed status in F1 subtypes (Supplemental Figure S20C, http://links.lww.com/HEP/H917). The cell-cell communication analysis demonstrated that there were more interactions between malignant and T cell subpopulations in F1 tumors (Supplemental Figure S20D, E, http://links.lww.com/HEP/H917).

We then applied the FAD classification to immunocompetent HCC mouse models. We established 2 models named NRAS.MYC.ND and NRAS.MYC.KD using the Sleeping Beauty transposon system to deliver MYC and NRASG12V constructs by means of hydrodynamic tail vein injections, then fed with normal diet or ketogenic diet, respectively. The expression pattern of FAD genes and contents of FFAs of these two models were validated by RNA-seq and lipidomics (Supplemental Figure S21A–C, http://links.lww.com/HEP/H917). The RNA-seq data sets of all 13 mouse models (11 from publicly available data sets) were combined and the batch effects were removed as shown by PCA analysis (Supplemental Figure S21D, E, http://links.lww.com/HEP/H917). The 98 mouse HCC samples were clustered into 3 subtypes (Figure 6A). Consistent with the findings that F1 and F3 were characterized by RAS and AKT signaling, respectively (Figure 3I, L, Supplemental Figure S22, http://links.lww.com/HEP/H917), the NRAS-induced model belonged to the F1 subtypes, while the AKT-driven model was a member of F3 subtypes (Figure 6A). F1 subtypes had much higher expression of CD8, cytotoxic, and exhausted T cells marker genes compared to F3 subtypes (Supplemental Figure S21F, http://links.lww.com/HEP/H917). We then selected 1 representative model for each subtype (Figure 6A). The F1 model had more infiltrated T cells, cytotoxic T cells, and exhausted T cells than F2 and F3 models (Figure 6B, C, Supplemental Figure S21G, http://links.lww.com/HEP/H917). Collectively, F1 subtypes exhibited a more substantial immune infiltration with immunosuppressive and exhaustive microenvironment compared to F2 and F3 subtypes.

We further validated the immune landscape of FAD subtypes using scRNA-seq with the F1 and F3 mouse HCC models (Figure 6D). Unsupervised t-SNE analysis of the total cells identified 24 subclusters (Supplemental Figure S23A, http://links.lww.com/HEP/H917), including macrophages, malignant cells, T cells, etc. (Figure 6E), in which the malignant cells were identified by copy number variation (Supplemental Figure S23B, http://links.lww.com/HEP/H917). F1 model was enriched with T cells, while F3 model was dominant with macrophages (Figure 6F, G, Supplemental Figure S23C, http://links.lww.com/HEP/H917). To further characterize the T cells phenotype, we subclustered the pooled T cells (Figure 6H) and annotated the clusters.[24] Four subpopulations were identified from the F1-derived T cells including progenitor, proliferating, effector-like, and terminally exhausted T cells, whereas all the F3-derived T cells were identified as progenitors (Figure 6I, J), which was validated by pseudotime analysis (Figure 6K). The progenitor, proliferating, effector-like, and terminally subpopulation of exhausted T cells highly expressed Tcf7, Mki67, Gzmk, and Tox, accordingly (Figure 6L). In agreement with the findings from human samples, the F1-derived T cells had much higher expression of cytotoxic and exhausted T cell markers than F3-derived T cells (Figure 6M, Supplemental Figure S23D, http://links.lww.com/HEP/H917). More intercellular communications were detected between malignant cells and T cell subpopulations in F1 than F3 tumors (Figure 6N, O, Supplemental Figure S23E, http://links.lww.com/HEP/H917). Pathway activity analysis revealed that the PD-L1 expression and PD-1 checkpoint pathway was significantly enriched between malignant cells and several T cell populations, indicating a PD-1/PD-L1-mediated immunosuppression in F1 tumors (Figure 6P).

FAD subtypes predict response to immune checkpoint inhibitor monotherapy and combinations

Considering the TME characteristics of FAD subtypes, we speculated that HCCs from F1 subtypes were

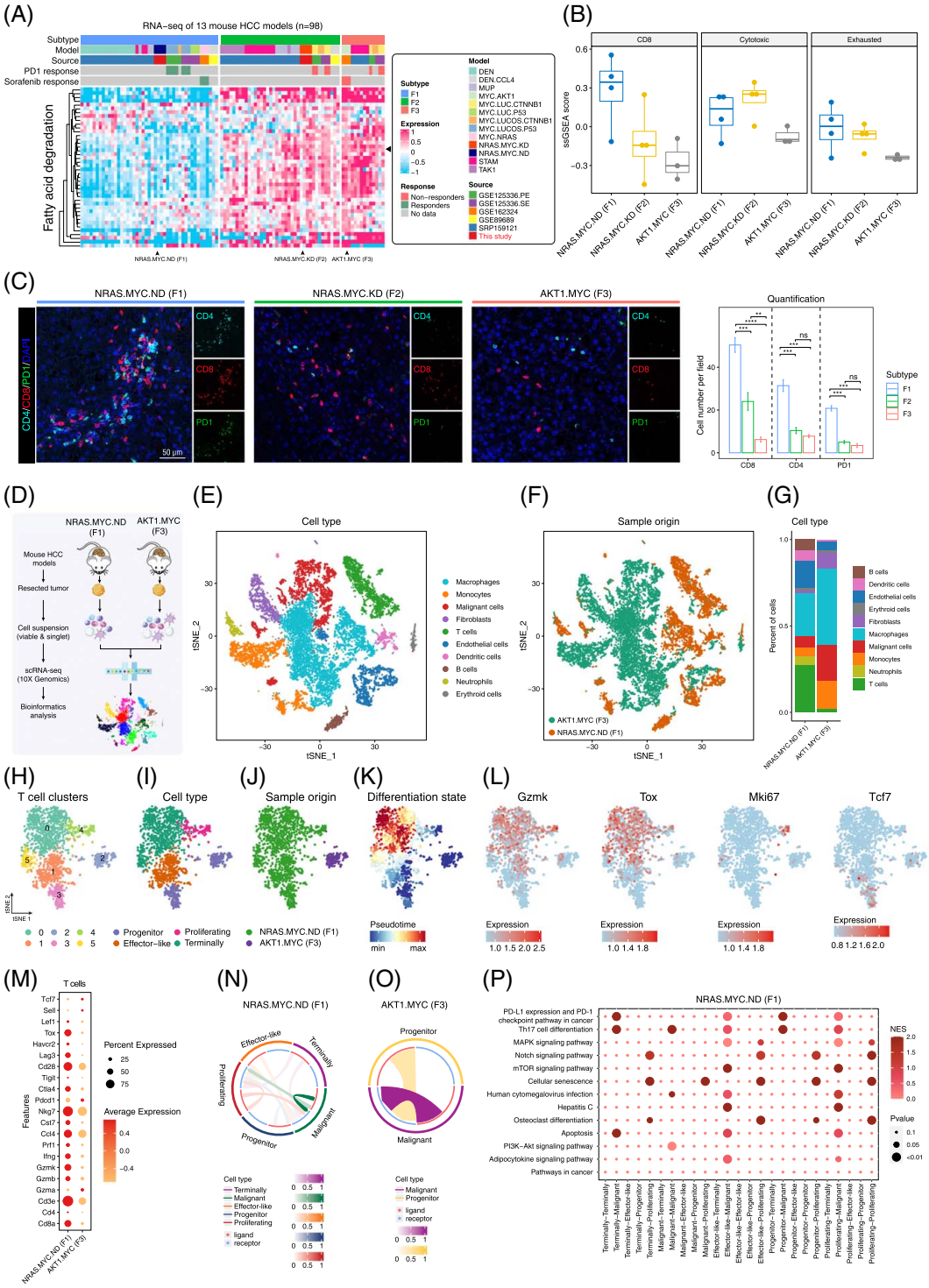

FIGURE 6 Characterization of the immune microenvironment of FAD subtypes in patients with HCC and mouse models. (A) Heatmap showing the identification of FAD subtypes in mouse HCC models. (B) ssGSEA score indicated the estimated contents of CD8, cytotoxic, and exhausted T cells in a representative F1, F2, and F3 model. (C) Multiplex immunohistochemistry (mIHC) staining of PD1, CD4, and CD8 cells from representative F1, F2, and F3 mouse HCC models. (D) Workflow of sample preparation, sequencing, and bioinformatic analysis. (E and F) t-SNE visualization of single cells profiled in this study with each cell color coded for cell type (E), and sample origin (F). (G) Barplot representing the percent of cells in each sample. (H–J) t-SNE plots of the cell clusters (H), cell type (I), and sample origin (J) of the T cells. (K) Trajectory plot showing the pseudotime of T cells in each exhausted T cell subpopulations. (L) t-SNE plot showing the expression level of marker gene for progenitor (Tcf7), effector-like (Gzmk), proliferating (Mki67), and terminally (Tox) exhausted CD8 T cell subpopulations. (M) Dot plot showing the expression pattern of T cell subpopulation markers in T cells derived from F1 and F3 mouse model. (N and O) The cell-cell interactions of malignant cells and T cells in mouse HCC models from F1 (N) and F3 (O) subtypes. (P) Bubble plot showing the pathway activity analysis involved in communications between indicated cell types in F1 subtypes. Abbreviation: FAD, fatty acid degradation.

candidates for immunotherapy. We noticed that the mouse HCC models from F1 subtypes were responsive to anti-PD1 therapy, while mouse models from F2 and F3 subtypes were nonresponders (Figure 6A). We generated mouse HCC models belonging to different subtypes, then subjected to anti-PD1 therapy (Figure 7A, Supplemental Figure S21A–C, http://links.lww.com/HEP/H917). The number of nodules and cell proliferation decreased after anti-PD1 therapy in F1 rather than F2 and F3 subtypes as measured by MRI, whole-liver morphology, and Ki-67 staining (Figure 7B). Accordingly, the F1 subtype mice showed a significant increase in survival after anti-PD-1 therapy compared to isotype controls (Figure 7C). In contrast, no therapeutic effect was observed in F2 and F3 models (Figure 7D, E). We further validated the findings in 2 other models, in which the MYC.sgTrp53 model (F1 subtype) was sensitive to anti-PD-1 therapy, while the MYC.CTNNB1-ΔN90 model (F3 subtype) was resistant to anti-PD-1 therapy (Supplemental Figure S24A, B, http://links.lww.com/HEP/H917). RNA-seq demonstrated the transcriptomic similarity between MYC/NRAS and MYC/sgTrp53 models as well as the similarity between MYC/CTNNB1-ΔN90 and MYC/AKT models, especially in the expression pattern of FAD gene (Supplemental Figure S24C, D, http://links.lww.com/HEP/H917).

To determine whether FAD subtypes can be used as a tool to predict response to immune checkpoint inhibitor (ICIs), we explored the associations between FAD subtypes and ICI response. As shown in Figure 2B, 77.8% (7/9) of the patients in F1 subtypes were PD1 responders, which was significantly higher than F2 and F3 whose ratio was 25% (1/4) and 0 (0/4), respectively ($p = 0.026$, Supplemental Table S9, http://links.lww.com/HEP/H917). Similar findings were observed in a Korean cohort ($p = 0.007$, Supplemental Figure S25A–C, http://links.lww.com/HEP/H917), which comprised 40 patients with HCC receiving anti-PD-1 therapy.[25] Considering the limited sample sizes of both cohorts, we combined these 2 cohorts and removed the batch effect (Supplemental Figure S25D, http://links.lww.com/HEP/H917). FAD subtypes were identified in the new cohort named “The Asian PD1 cohort” (Figure 7F). F1 subtypes had the highest anti-PD1 response rate (61.1%) compared to F2 (14.3%) and F3 (0%) ($p < 0.001$, Figure 7G). FAD score achieved good performance in predicting anti-PD1 response with an AUC of 0.855 (Figure 7H). A complete regression of tumors was observed in one F1 patient, while the tumor progressed after 20 weeks of anti-PD1 therapy in one F3 patient (Figure 7I, J, Supplemental Figure S25E, http://links.lww.com/HEP/H917). The mIHC staining showed that the infiltrated CD8 T cells and the PD-1 expression were much higher in patient PT1 than PT4 (Supplemental Figure S25F, http://links.lww.com/HEP/H917).

We also examined the potential usage of FAD subtypes in predicting response to anti-PD-L1 monotherapy. The FAD subtypes were applied to GO30140 group F cohort,[26] in which the F1 subtypes had higher response rate than other 2 subtypes (Figure 7K). Atezolizumab responders had lower FAD scores than nonresponders (Figure 7L), indicating FAD subtypes are associated with anti-PD-L1 monotherapy response.

We further subclustered the T + A cohort with FAD classifier (Supplemental Figure S26A, http://links.lww.com/HEP/H917). Patients in F2 subtypes showed improved OS and PFS when treated with T + A versus sorafenib, whereas patients in F3 showed no difference in OS and PFS (Supplemental Figure S26B, http://links.lww.com/HEP/H917). The response of F1 subtypes was not assessable due to the limited sample size of patients treated with sorafenib patients (Supplemental Figure S26B, http://links.lww.com/HEP/H917). Thus, we further explored the relationship between FAD score and T + A response. Low FAD score (defined by median split) was associated with improved PFS and OS with T + A versus sorafenib, whereas patients with high FAD score showed no difference in PFS and OS (Figure 7M). F1 subtypes that had the worst prognosis in treatment-naive cohorts exhibited the best OS and PFS (Figure 7N), indicating the benefit of F1 patients from T + A treatment.

FAD subtype-specific serum biomarkers and therapeutic strategies for HCC

Liver biopsy is not mandatory for the diagnosis of HCC, which might hamper the translation of FAD subtypes to the clinic. Therefore, we further performed metabolomics and proteomics examinations with the pretreatment serum samples from our cohort (n = 41). The subtype-specific serum metabolites were identified using a method as described[23] (Figure 8A). The 20 blood-based metabolites could diagnose F1, F2, and F3 subtypes with AUC of 0.984, 0.75, and 0.879, respectively (Figure 8B). The blood-based proteomics also identified 20 subtype-specific proteins (Figure 8C), which predicts F1, F2, and F3 subtypes with AUC of 0.932, 0.827, and 0.884, respectively (Figure 8D). In agreement with the genomic analysis, AFP and SPP1 were identified as serum biomarkers for F1 subtypes (Supplemental Figure S13B, http://links.lww.com/HEP/H917). Subsequently, the subtype prediction was repeated with the proteomic and metabolomic classifiers. The liquid biopsy signatures can reproducibly determine the FAD subtypes and predict the response to anti-PD1 therapy in our cohort (Supplemental Figure S27, http://links.lww.com/HEP/H917). In conclusion, the metabolite and protein signature in peripheral blood could discriminate FAD subtypes with high accuracy and sensitivity.

In this study, we identified a novel FAD subtype of HCC based on multiomics and explored the clinical,

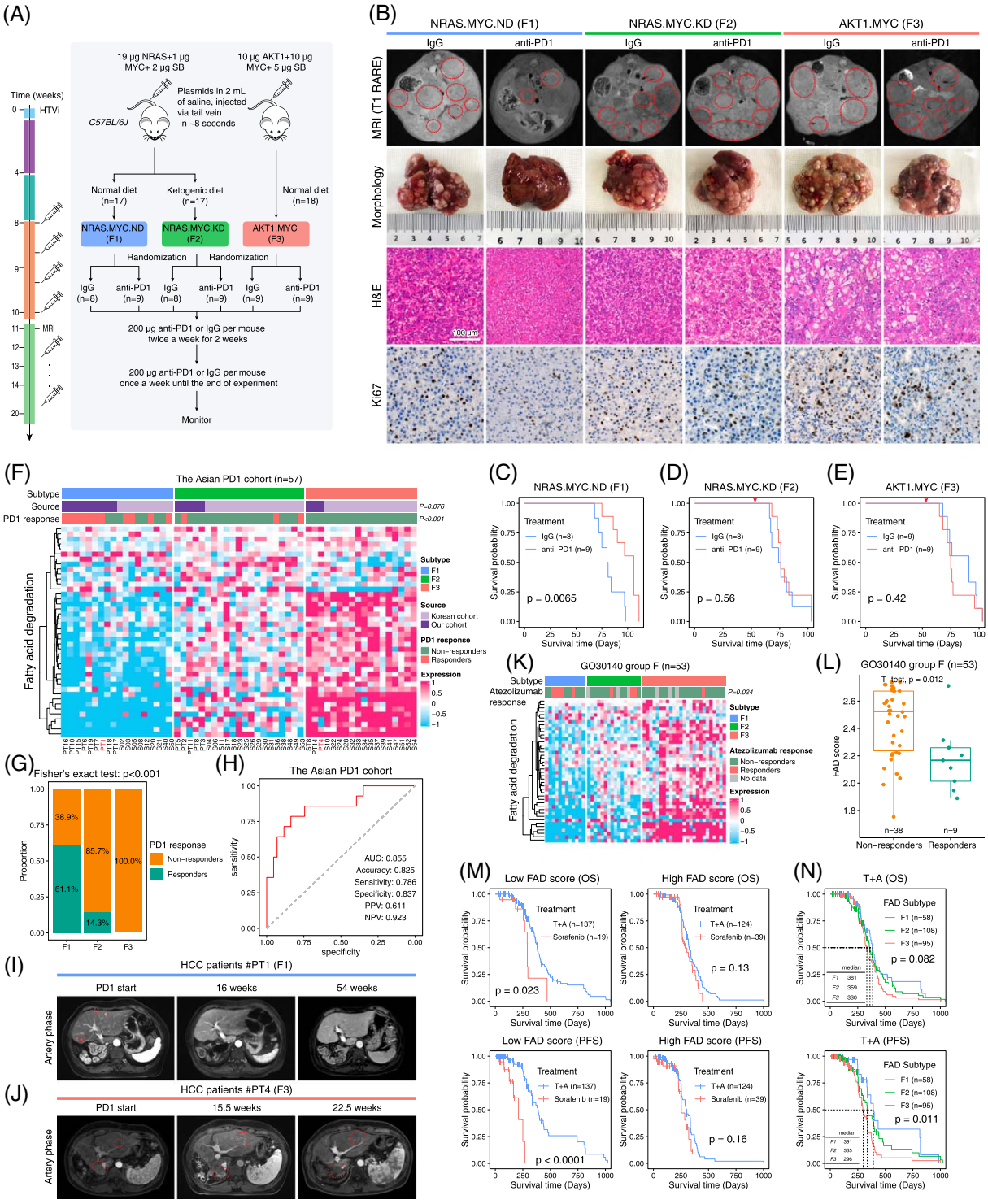

FIGURE 7 FAD subtypes predict response to ICI monotherapy and combinations. (A) Schematic diagram for the establishment of mouse models and treatment procedure. (B) Representative images of MRI, whole-liver morphology, H&E, and Ki-67 staining of sections from IgG or PD-1-treated mice from F1, F2, and F3 mouse HCC models. The dotted circles indicated tumors. (C–E) Survival curves of IgG and PD1-treated mice from F1 (C), F2 (D), and F3 (E) mouse HCC models. (F) Heatmaps showing the FAD subtypes and anti-PD-1 response in the Asian PD1 cohort. (G) The percentage of PD-1 responders and nonresponders across FAD subtypes in the Asian PD-1 cohort. (H) AUC showing the performance of the FAD score in predicting PD-1 response in the Asian PD-1 cohort. (I and J) MRI scans of a responder (I) and a nonresponder (J) patient to camrelizumab, before and after treatment. (K) Heatmaps showing the FAD subtypes in patients receiving anti-PD-L1 (atezolizumab) monotherapy. (L) Boxplot showing the FAD score in anti-PD-L1 responders and nonresponders. (M) Kaplan-Meier plots of OS and PFS in EGAD00001008128 stratified by treatment in patients with high or low (split by median) FAD scores. (N) Kaplan-Meier curves of OS and PFS in patients receiving T+A treatment stratified by FAD subtypes. Abbreviations: FAD, fatty acid degradation; ICI, immune checkpoint inhibitor; PD-1, programmed cell death-1.

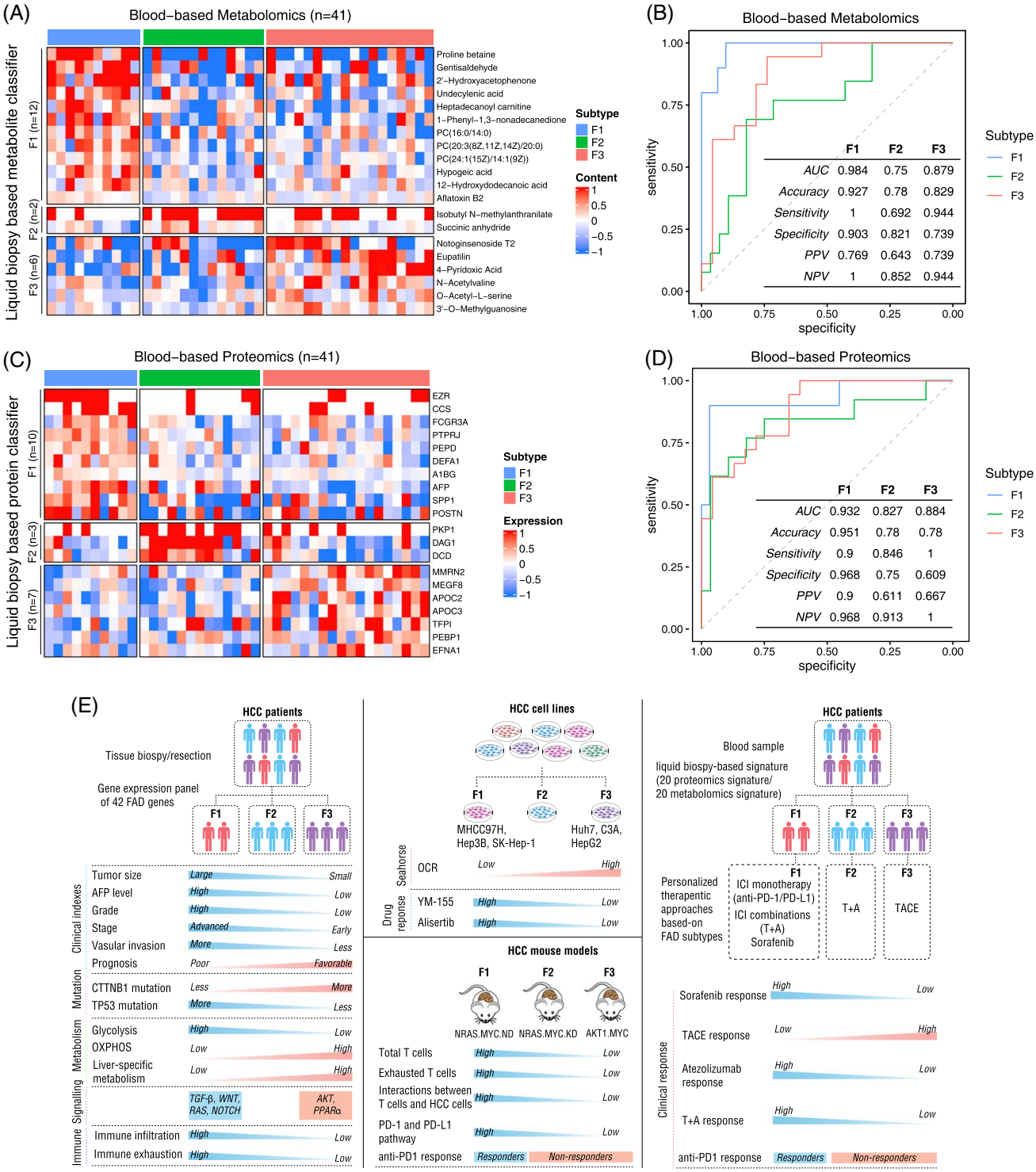

FIGURE 8 FAD subtype-specific serum biomarkers and therapeutic strategies for HCC. (A) Heatmap of the serum metabolite levels specific to FAD subtypes in patients with HCC based on metabolomics. (B) AUC showing the performance of the liquid biopsy–based metabolomic classifier in capturing the FAD subtypes. (C) Heatmap of the serum protein levels specific to FAD subtypes in patients with HCC based on proteomics. (D) AUC showing the performance of the liquid biopsy–based proteomic classifier in capturing the FAD subtypes. (E) Summary of the FAD subtypes of HCC and the FAD subtype-based personalized treatment strategies. Abbreviations: FAD, fatty acid degradation; ICI, immune checkpoint inhibitor; PD-1, programmed cell death-1.

genomic, epigenetic, metabolic, and immunological characteristics. The FAD subtypes might implement personalized medicine for the clinical management of HCC, in which F1 subtypes represent responders to sorafenib and immune checkpoint inhibitor monotherapy or combinations, while F3 subtypes are responders to TACE. The F2 subtypes, the intermediate status between F1 and F3, are potential responders to T + A.

We also identified the preclinical drugs YM-155 and Alisertib as F1-specific drugs. Finally, we propose a liquid biopsy–based diagnostic algorithm that aims to implement the FAD subtypes in clinical practice (Figure 8E).

DISCUSSION

Molecular classification contributes to a better understanding of the heterogeneity of HCC and developing personalized therapy.[2] Multiple molecular classifications of HCC have been proposed in recent years, from which it is well established that HCC can be reproducibly classified into several molecular subclasses with distinct phenotypes based on the genomic or transcriptomic profiling.[27] However, there remains a substantial gap in translating subtypes into clinical practice due to the limited sample size, high classifier complexity, and the unmet needs for guiding therapeutic decision-making. The F3 subtypes overlapped with CTNNB1 subtype in both Chiang and Lachenmayer classification, which was consistent with the finding that F3 subtypes had higher mutational rate of CTNNB1 and indicated F3 subtypes may benefit from Wnt signaling pathway-targeted inhibitors. We found that F3 subtypes lacked a T-cell–inflamed tumor microenvironment, which agreed with the reports that WNT/β-catenin pathway activation correlates with immune exclusion and promotes resistance to anti-PD-1 therapy.[28] Since F2 subtypes had the highest GPC3 expression, it is encouraging to explore whether GPC3-targeting strategies such as chimeric antigen receptor (CAR)-T, antibody, and vaccine therapy will be more effective for F2 patients in the future.

Here, we provided a link between FA content in TME and immunotherapy response. The F1 subtypes had lower FAD activity, which caused the accumulation of FAs in the microenvironment. Several studies have focused on the effect of FFAs on T cells, in which the overall data suggested that low concentrations of FFAs can influence the proliferation of T cells, whereas higher concentrations induce apoptosis in a dose-dependent manner.[29] Accumulation of FAs in the TME drives dysfunction in intratumoral CD8+ T cells through lipotoxicity, and dampens their ability to control tumor progression.[30] Since promoting FA catabolism of CD8 T cells improves their ability to combat tumors,[31] it will be interesting to see whether selective activation of FA utilization in T cells would enhance the antitumor immune response in F1 subtypes.

TACE is recommended for intermediate-stage patients with HCC. However, indicators for TACE response need to be determined. Here, we found that F3 subtypes exhibited higher response rate than F1, although doxorubicin, a chemotherapeutic agent injected into the hepatic artery in TACE, presented higher efficiency in F1 patients (Supplemental Figure S16A, http://links.lww.com/HEP/H917). One plausible explanation for the seemingly contradictory finding is that F3 tumors were more dependent on OXPHOS (Figure 3G, H). TACE loads both chemotherapeutic and hypoxic stress on cancer cells. The F1 patients with high glycolysis and HIF activity may already be hypoxic prior to TACE (Figures 3F, I, L). Hypoxia response may cause TACE resistance.[32] Further study is warranted to clarify the precise mechanism of TACE resistance in F1 subtypes.

Sorafenib is the standard systemic therapy for advanced HCC, yet potential predictive biomarkers and mechanisms of response or resistance to sorafenib have not been extensively identified. We demonstrated that FAD subtypes were predictive to sorafenib efficacy in PDX models and patient cohorts, thus linked FA metabolism and sorafenib response. Recent research has suggested that sorafenib-mediated lipotoxicity contributes to its therapeutic efficacy, in which sorafenib acts as a direct LXR signaling activator and promotes liponeogenesis and a toxic accumulation of saturated FAs.[33] In patients with high FAD activity, the FAs could be oxidized thus the lipotoxic effects could be reduced, which explains why F3 subtypes are sorafenib nonresponders. In addition, we found that sorafenib treatment results in a switch from F1 to F3 subtypes in vitro and in vivo, which partly explains the mechanism of sorafenib resistance in patients with HCC and highlights the sequential or combination therapies of sorafenib and TACE.

Several limitations to this study need to be acknowledged. First, most of our cohorts were retrospective. Second, we provide preliminary evidence that the FAD subtypes can be diagnosed based on liquid biopsies. Additional liquid biopsy–based cohorts with therapeutic response data available will be more helpful. Third, we linked FAD subtypes with several first-line therapies to HCC. The precise underlying molecular mechanisms remain to be elucidated. A recently published article by Murai and colleagues demonstrated that intratumor steatosis may be a useful noninvasive imaging biomarker for predicting the efficacy of T + A therapy. Mechanically, the intratumoral lipid accumulation induced immunosuppression in macrophages and fibroblasts through PD-L1 upregulation in steatotic patients with HCC.[34] Overall, the study here and the work led by Murai and colleagues are complementary to each other. FAD subtypes are stable in their nonviral cohort and linked to class I/II/III (Supplemental Figure S9H, http://links.lww.com/HEP/H917). Murai and colleagues concluded that steatotic HCC (supposed to be class II) may be ideal candidates for T + A therapy from a very small cohort ($n = 30$), which is consistent with our findings that F2 subtypes are responsive to T + A therapy from a large sample size ($n = 261$). In addition, the mechanism proposed by them that lipid accumulation induced immunosuppression can partly explain the immune-enriched but immune-exhausted TME in F1 subtypes.

In summary, we defined a FAD classification of HCC through multiomics analysis and proposed a personalized treatment algorithm based on FAD subtypes. Further investigations in larger prospective cohorts are warranted to determine the potential utilization of FAD subtypes for personalized therapy in HCC.

DATA AVAILABILITY STATEMENT

Transcriptomic data are available at the Gene ExpressionOmnibus (GSE202069, GSE202070,GSE202071). Previously published data sets analyzed in this study are indicated in online Supplemental Table S3, http://links.lww.com/HEP/H916. Other data are available on reasonable request.

AUTHOR CONTRIBUTIONS

Binghua Li, Wajahat Z. Mehal, and Decai Yu developed the study concept; Decai Yu and Wajahat Z. Mehal supervised the project. Binghua Li performed the computational analysis; Binghua Li, Yunzheng Li, Liyuan Qian, Yanchao Xu, Huan Li, Yuanyuan Xie, Ye Wang, Yijun Lu, Zhu Xu, Yuchen Zhang, and Qi Liu conducted experiments; Jin Peng, Chunxiao Cheng, Ke Su, and Laizhu Zhang collected the clinical data; Jin Peng, Yajuan Cao, Jiaming Lu, and Decai Yu managed the patients and assessed the clinical response; Binghua Li and Yue Hu contributed biopsy samples and pathology analysis. Huajun Zhou and Sheng Guo performed the PDX experiment and data analysis. Binghua Li and Decai Yu wrote the manuscript with the help of Wajahat Z. Mehal. All authors read and approved the final version of the manuscript.

ACKNOWLEDGMENTS

The authors thank the patients and investigators who participated in the publicly available data sets for providing data. The authors thank the assistance from Shanghai Biotree Biotech Co. Ltd., Hangzhou LC-bio, Beijing Novogene Co. Ltd., and Shanghai Wcgene Biotech for the support of high-throughput technologies. Binghua Li would like to thank Dr. Zuguang Gu for his assistance with the ComplexHeatmap plot.

FUNDING INFORMATION

This work was supported by grants from the National Natural Science Foundation of China (No. 82002509, 82173129, 81871967, 82103384, and 82103453), China Postdoctoral Science Foundation (No.2019M661803), Social Development Foundation of Jiangsu Province of China (No. BE2018604), Jiangsu Provincial Medical Talent, the Special Fund of Nanjing Health Science and Technology Development (No. YKK21079), the Start-up Funding for Talent Introduction of Drum Tower Hospital (RC2023-032), and the Fundings for Clinical Trials from the Affiliated Drum Tower Hospital, Medical School of Nanjing University (2021-LCYJ-MS-12).

CONFLICTS OF INTEREST

Wajahat Mehal consults for Pfizer. The remaining authors have no conflicts to report.

ORCID

Binghua Li https://orcid.org/0000–0001–7209–2854
Yunzheng Li https://orcid.org/0000–0002–4541–1909
Huajun Zhou https://orcid.org/0000–0002–8600–0727
Yanchao Xu https://orcid.org/0000–0002–1112–6026
Yajuan Cao https://orcid.org/0000–0002–8683–123X
Chunxiao Cheng https://orcid.org/0000–0002–4696–0520
Jin Peng https://orcid.org/0000–0003–1660–3271
Huan Li https://orcid.org/0000–0002–9254–3904
Laizhu Zhang https://orcid.org/0000–0002–9582–4357
Ke Su https://orcid.org/0000–0002–5776–3987
Zhu Xu https://orcid.org/0000–0002–8057–7111
Yue Hu https://orcid.org/0000–0002–9240–6483
Jiaming Lu https://orcid.org/0000–0002–7622–4233
Yijun Lu https://orcid.org/0000–0001–7414–6406
Liyuan Qian https://orcid.org/0000–0002–3229–1100
Ye Wang https://orcid.org/0000–0003–0936–5156
Yuchen Zhang https://orcid.org/0009–0008–8122–6218
Qi Liu https://orcid.org/0000–0002–5576–8469
Yuanyuan Xie https://orcid.org/0000–0002–1019–5070
Sheng Guo https://orcid.org/0000–0002–9346–0457
Wajahat Z. Mehal https://orcid.org/0000–0001–8481–3671
Decai Yu https://orcid.org/0000–0002–3006–2531

REFERENCES

1. Llovet JM, Kelley RK, Villanueva A, Singal AG, Pikarsky E, Roayaie S, et al. Hepatocellular carcinoma. Nat Rev Dis Primers. 2021;7:6.
2. Rebouissou S, Nault J-C. Advances in molecular classification and precision oncology in hepatocellular carcinoma. J Hepatol. 2020;72:215–9.
3. Shimada S, Mogushi K, Akiyama Y, Furuyama T, Watanabe S, Ogura T, et al. Comprehensive molecular and immunological characterization of hepatocellular carcinoma. EBioMedicine. 2019;40:457–70.
4. Sia D, Jiao Y, Martinez-Quetglas I, Kuchuk O, Villacorta-Martin C, de Moura MC, et al. Identification of an immune-specific class of hepatocellular carcinoma, based on molecular features. Gastroenterology. 2017;153:812–26.
5. Cancer Genome Atlas Research Network. Electronic address wbe, wheeler@bcm.edu; Cancer Genome Atlas Research Network. Comprehensive and integrative genomic characterization of hepatocellular carcinoma. Cell. 2017;169:1327–41 e1323.
6. Gao Q, Zhu H, Dong L, Shi W, Chen R, Song Z, et al. Integrated proteogenomic characterization of HBV-related hepatocellular carcinoma. Cell. 2019;179:561–77.
7. Jiang Y, Sun A, Zhao Y, Ying W, Sun H, Yang X, et al. Proteomics identifies new therapeutic targets of early-stage hepatocellular carcinoma. Nature. 2019;567:257–61.
8. Bidkhori G, Benfeitas R, Klevstig M, Zhang C, Nielsen J, Uhlen M, et al. Metabolic network-based stratification of hepatocellular carcinoma reveals three distinct tumor subtypes. Proc Natl Acad Sci U S A. 2018;115:E11874–83.
9. Pavlova NN, Thompson CB. The emerging hallmarks of cancer metabolism. Cell Metab. 2016;23:27–47.

10. Currie E, Schulze A, Zechner R, Walther TC, Farese RV Jr. Cellular fatty acid metabolism and cancer. Cell Metab. 2013;18:153–61.
11. Wanders RJA, Komen J, Kemp S. Fatty acid omega-oxidation as a rescue pathway for fatty acid oxidation disorders in humans. FEBS J. 2011;278:182–94.
12. Wang M, Han J, Xing H, Zhang H, Li Z, Liang L, et al. Dysregulated fatty acid metabolism in hepatocellular carcinoma. Hepatic Oncol. 2016;3:241–51.
13. Senni N, Savall M, Cabrerizo Granados D, Alves-Guerra MC, Sartor C, Lagoutte I, et al. beta-catenin-activated hepatocellular carcinomas are addicted to fatty acids. Gut. 2019;68:322–4.
14. Reig M, Forner A, Rimola J, Ferrer-Fábrega J, Burrel M, Garcia-Criado Á, et al. BCLC strategy for prognosis prediction and treatment recommendation: the 2022 update. J Hepatol. 2022;76:681–93.
15. Finn RS, Qin S, Ikeda M, Galle PR, Ducreux M, Kim T-Y, et al. Atezolizumab plus bevacizumab in unresectable hepatocellular carcinoma. N Engl J Med. 2020;382:1894–905.
16. Li B, Xu T, Liu C, Meng G, Sun Y, Qian L, et al. Liver-enriched genes are associated with the prognosis of patients with hepatocellular carcinoma. Sci Rep. 2018;8:11197.
17. Hoshida Y, Toffanin S, Lachenmayer A, Villanueva A, Minguez B, Llovet JM. Molecular classification and novel targets in hepatocellular carcinoma: recent advancements. Semin Liver Dis. 2010 ;30:35–51.
18. Chiang DY, Villanueva A, Hoshida Y, Peix J, Newell P, Minguez B, et al. Focal gains of VEGFA and molecular classification of hepatocellular carcinoma. Cancer Res. 2008;68:6779–88.
19. Lachenmayer A, Alsinet C, Savic R, Cabellos L, Toffanin S, Hoshida Y, et al. Wnt-pathway activation in two molecular classes of hepatocellular carcinoma and experimental modulation by sorafenib. Clin Cancer Res. 2012;18:4997–5007.
20. Boyault S, Rickman DS, De Reyniès A, Balabaud C, Rebouissou S, Jeannot E, et al. Transcriptome classification of HCC is related to gene alterations and to new therapeutic targets. Hepatology. 2007;45:42–52.
21. Lee JS, Chu IS, Heo J, Calvisi DF, Sun Z, Roskams T, et al. Classification and prediction of survival in hepatocellular carcinoma by gene expression profiling. Hepatology. 2004;40:667–76.
22. Coulouarn C, Factor VM, Thorgeirsson SS. Transforming growth factor-β gene expression signature in mouse hepatocytes predicts clinical outcome in human cancer. Hepatology. 2008;47:2059–67.
23. Lee SH, Yim SY, Jeong YS, Li QX, Kang SH, Sohn BH, et al. Consensus subtypes of hepatocellular carcinoma associated with clinical outcomes and genomic phenotypes. Hepatology. 2022;76:1634–48.
24. Miller BC, Sen DR, Al Abosy R, Bi K, Virkud YV, LaFleur MW, et al. Subsets of exhausted CD8(+) T cells differentially mediate tumor control and respond to checkpoint blockade. Nat Immunol. 2019;20:326–6.
25. Hong JY, Cho HJ, Sa JK, Liu X, Ha SY, Lee T, et al. Hepatocellular carcinoma patients with high circulating cytotoxic T cells and intra-tumoral immune signature benefit from pembrolizumab: results from a single-arm phase 2 trial. Genome medicine. 2022;14:1–15.
26. Zhu AX, Abbas AR, de Galarreta MR, Guan Y, Lu S, Koeppen H, et al. Molecular correlates of clinical response and resistance to atezolizumab in combination with bevacizumab in advanced hepatocellular carcinoma. Nature Medicine. 2022;28:1–13.
27. Goossens N, Sun X, Hoshida Y. Molecular classification of hepatocellular carcinoma: potential therapeutic implications. Hepatic Oncol. 2015;2:371–9.
28. de Galarreta MR, Bresnahan E, Molina-Sánchez P, Lindblad KE, Maier B, Sia D, et al. β-catenin activation promotes immune escape and resistance to anti-PD-1 therapy in hepatocellular carcinoma. Cancer Discov. 2019;9:1124–41.
29. de Jong AJ, Kloppenburg M, Toes REM, Ioan-Facsinay A. Fatty acids, lipid mediators, and T-cell function. Front Immunol . 2014;5:483.
30. Manzo T, Prentice BM, Anderson KG, Raman A, Schalck A, Codreanu GS, et al. Accumulation of long-chain fatty acids in the tumor microenvironment drives dysfunction in intrapancreatic CD8+T cells. J Exp Med. 2020;217:e20191920.
31. Zhang Y, Kurupati R, Liu L, Zhou XY, Zhang G, Hudaihed A, et al. Enhancing CD8+T cell fatty acid catabolism within a metabolically challenging tumor microenvironment increases the efficacy of melanoma immunotherapy. Cancer Cell. 2017;32:377–91.
32. Fako V, Martin SP, Pomyen Y, Budhu A, Chaisaingmongkol J, Franck S, et al. Gene signature predictive of hepatocellular carcinoma patient response to transarterial chemoembolization. Int J Biol Sci. 2019;15:2654–63.
33. Rudalska R, Harbig J, Snaebjornsson MT, Klotz S, Zwirner S, Taranets L, et al. LXRα activation and Raf inhibition trigger lethal lipotoxicity in liver cancer. Nature Cancer. 2021;2:201–17.
34. Murai H, Kodama T, Maesaka K, Tange S, Motooka D, Suzuki Y, et al. Multiomics identifies the link between intratumor steatosis and the exhausted tumor immune microenvironment in hepatocellular carcinoma. Hepatology. 2023;77:77–91.

How to cite this article: Li B, Li Y, Zhou H, Xu Y, Cao Y, Cheng C, et al. Multiomics identifies metabolic subtypes based on fatty acid degradation allocating personalized treatment in hepatocellular carcinoma. Hepatology. 2024;79:289–306. https://doi.org/10.1097/HEP.0000000000000553